EXPERIMENTAL ANALYSIS OF THE FIXED FLAT-PLATE SOLAR COLLECTOR WITH Sn-AL_2O_3 SELECTIVE ABSORBER AND GRAVITY WATER FLOW

by

Aleksandar M. NEŠOVIĆ[a*], Nebojša S. LUKIĆ[a], Nebojša M. JURIŠEVIĆ[a], Dragan Z. CVETKOVIĆ[b], Dragan S. DŽUNIĆ[a], Mladen M. JOSIJEVIĆ[a], and Bogdan P. NEDIĆ[a]

[a] Faculty of Engineering, University of Kragujevac, Kragujevac, Serbia
[b] Institute of Information Technologies, University of Kragujevac, Kragujevac, Serbia

Original scientific paper
https://doi.org/10.2298/TSCI220904171N

To improve solar collector efficiency, a variety of designs and materials have been introduced into production practice. Studies describing solar collector specifics, therefore, are particularly valuable to the scientific community as they contribute to the overall body of knowledge and constant improvement the in the scientific field. In that regard, the study presented in this paper analyses the thermal performance of the fixed flat-plate collector with an Sn-Al_2O_3 selective absorber. The fixed flat-plate collector design utilizes gravity water flow in an open loop system. A two-month study was conducted to perform the analysis. The experiment was based on measurements of water flow in the fixed flat-plate collector, the water temperature at the fixed flat-plate collector inlet and outlet, and solar radiation intensity on a horizontal surface. Results for three randomly selected measurement days have shown that fixed flat-plate collector can achieve relatively satisfactory values for average daily specific heat power, thermal efficiency, and inlet-outlet water temperature gradient, respectively: June 29 (381.78 W/m^2, 60.67%, and 9.06 °C), June 30 (364.33 W/m^2, 59.43%, and 7.46 °C), and July 15 (373.06 W/m^2, 59.85%, and 8.69 °C). Apart from the relatively good measurement results, this type of solar collector does not require circulating pumps for operation, which brings a double advantage: energy saving and energy production.

Key words: *fixed flat-plate solar collector, Sn-Al_2O_3 selective absorber, gravity water flow, experimental model*

Introduction

The buildings and building construction sectors together account for 30% of global final energy consumption and 27% of total energy sector emissions [1]. In addition, global energy demand in the building sector is expected to increase by more than 50% between 2010 and 2050 [2]. For this reason, future strategies for the sustainable development of countries and regions will pay special attention to energy consumption in buildings. Considering that about 14% of household energy consumption is related to water heating [3], it can be assumed that diversification of water heating sources by the use of renewable energy, will be the focus

* Corresponding author, e-mail: aca.nesovic@kg.ac.rs

of future sustainable agendas. Apart from that, the energy produced by the use of solar collectors (SC) is constantly increasing [4].

This increase is largely due to the use of fixed flat-plate sollar collector (fFPSC), which are popular in the market. The reasons for their wide use are: a relatively simple and technological manufacturing process, relatively low price, lightweight, small thickness, high market availability, a wide range of applications (residential [5], industrial [6], *etc.*), and satisfactory thermal performance, thermal efficiency 40-80% [7].

To meet all of the mentioned criteria, Al and various selective coatings are used extensively in the manufacture of fFPSC absorber plates (Ni-Al_2O_3 [8-10], AlNi-Al_2O_3 [11], Mo-Al_2O_3 [12, 13], W-Al_2O_3 [14], Cu-$CuAl_2O_4$ [15], Pt-Al_2O_3 [16], Ag-Al_2O_3 [17], and Sn-Al_2O_3 [18-20]).

Deng *et al.* presented in [21] an FPSC with flat Al plates using micro heat pipes sputtered with a selective coating and placed in a closing space in the SC box. The advantages of this design are higher frost resistance, higher heat transfer coefficient, lower heat losses, elimination of the welding process, and prevention of leakage. The average daily thermal efficiency of the mentioned SC design during the three experimental days was: 71.05%, 64.25%, and 50.46%.

An example of an Al absorber with triangular flow channels in fFPSC is presented in [22]. The research results showed that this way, the optical and thermal efficiencies can be improved by 15.8% and 10.7%, respectively. Bezaatpour and Rostamzadeh made a relatively interesting proposal to reduce heat loss in SC by using Fe_3O_4-water nanofluid [23]. The results of their research showed that in this way and by rotating the tube inside the Al absorber, the heat losses of the FPSC are reduced by 1.65% to 10.44%. To increase the application of solar systems, Seddaoui *et al*. developed an SC with an Al absorber that combines the performance of an FPSC and an evacuated tube solar collector (ETSC) [24]. Experimental (as well as theoretical) models showed that this SC concept gives better results than FPSC (for 7.13%) and ETSC (for 28.32%). The air layer between the absorber and the glazing in fFPSC with an Al absorber was the subject of the analysis [25]. If the air layer were divided into two separate zones (using vertical partitions, *i.e.* barriers), the heat losses would be reduced by 2.2%. If there were three barriers, the same parameter would be reduced even more (by 5.3%). However, if the air layer were divided into four barriers, heat losses would increase by 2.9%. Paiva Garcia *et al*. concluded that the use of barriers in FPSC can be an excellent technical solution, but their number must be optimized depending on the specifics of the FPSC constructions.

In addition to studies describing the thermal performance of SC with Al absorbers, there are several studies describing the thermal performance of SC with natural circulation. Eltaweel *et al.* in [26] investigated the performance of the indirect thermosiphon fFPSC based on a heat exchanger with twisted tubes filled with a nanofluid. The results showed that the twisted tube heat exchanger system outperformed the circular tube heat exchanger by 12.8% (when the working fluid in the center SC is water) and by 12.5% (when the working fluid in the center SC is MWCNT-water nanofluid). The performance of copper oxide-water (CuO-water) nanofluid in FFPSC under natural and forced circulations was presented in [27]. The authors observed a significant improvement in performance under thermosyphon circulation compared to forced circulation. The CuO-water nanofluid was prepared with the inclusion of the surfactant sodium dodecylbenzene sulfonate (SDBS), Prasad and Chandra developed a theoretical model to determine the natural flow velocity through fFPSC and fFPSC heat losses [28]. The governing equations were expressed in terms of Grashof (Gr) and Prandtl (Pr) numbers and a dimensionless heat loss parameter. The method calculates the optimal inclination of the FPSC for a given latitude and insolation. The study presented in [29] dealt with the numerical analysis of natural convection heat transfer inside the SC. The SC with corrugated and flat absorbers were compared. The results were presented using streamlines, isotherms, and local and average Nusselt numbers. It was found that the flow and heat fields are affected by the shape of the enclosure and that the heat transfer rate is higher in the case of a corrugated than in the case of a flat enclosure. From the technical-economic point of view, the use of solar technologies has been justified in residential (solar power plant in the city of Askary – Turkey [30]) and in industry sectors, drying plants [31], sugar factories [32], *etc.*.

To contribute to the overall scientific body in this field, this paper analyses the thermal performance of a fFPSC with a selective Sn-Al_2O_3 absorber using gravity water flow in an open loop system. The experimental investigation was conducted on the territory of Central Serbia (Kragujevac city), where the moderate continental climate is predominant, and where significant amounts of final energy can be saved.

Materials

Fixed flat-plate solar collector

Construction details of the investigated fFPSC, fig. 1, with external dimensions of 965 × 475 × 80 mm, are simple, tab 1. The top of the absorber is single-glazed, while on the bottom there is hard-pressed mineral wool. The absorber consists of five selectively coated Sn-Al_2O_3 absorber plates. The internal hydraulic circuit consists of copper pipes with the following diameters: Ø22 × 1 mm (splitter/mixer) and Ø15 × 1 mm (flow channels in the absorber plates).

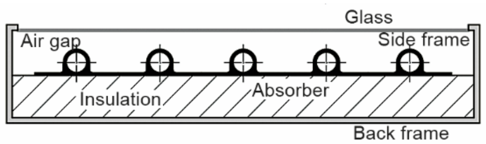

Figure 1. Cross-section of the fFPSC (transverse plane)

Table 1. Thermal characteristic of the fFPSC

Layer	Material	A [m^2]	δ [mm]	k [Wm^{-1}K^{-1}]	τ [–]	α [–]	ε [–]
Edges	Aluminum	0.23	2	203	–	–	–
Absorber[a,b]	Sn-Al_2O_3	0.35	2	203	–	0.88	0.25
Gas	Air	–	33.5	0.026	–	–	–
Cover	Glass	0.46	4	0.8	0.9	–	0.9
Insulation	Hard-pressed mineral wool	0.46	40	0.037	–	–	–

Note: a – One flat absorber plate dimension: 800 × 88 mm and b – Axial distance between flow channels: 88 mm

Solar installation

The experiment was conducted on the flat roof of the Faculty of Engineering, University of Kragujevac, Central Serbia, fig. 2.

The structure of the fFPSC – 1 is hinged to the stable pedestal – 3 and oriented southward over the bearing frame – 2. The joint – 4 allows the fFPSC to rotate around the E-W axis, while the threaded rods – 5 are used to precisely adjust the angle of inclination to the horizontal (the optimal angle β = 34° for the desired location is determined according to the

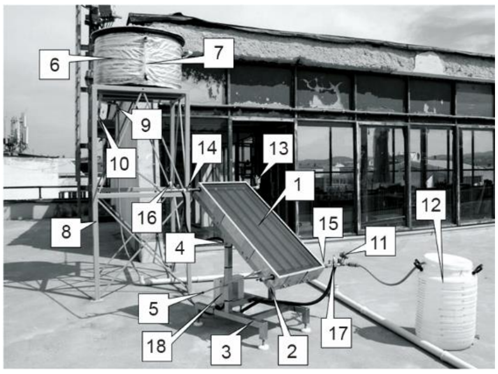

Figure 2. Isometric view of the solar installation with the fFPSC; *1 – fFPSC, 2 – fFPSC bearing frame, 3 – fFPSC stable pedestal, 4 – articulated joint, 5 – threaded rods, 6 – upper water tank, 7 – water level meter, 8 – upper water tank truss, 9 – discharge valve, 10 – stop valve, 11 – manual control valve, 12 – lower water tank, 13 – automatic air vent boiler, 14 and 15 – ball valves, 16 and 17 – pt-100 probes, and 18 – electrical cabinet*

recommendations by [33]. The upper water tank – 6, with a diameter of 800 mm and a volume of 250 L, has a built-in float inside to maintain the desired water level, which is read on the water level meter – 7 on the outside. The tank – 6, which stands on a tank truss – 8 with a height of 1800 mm, has two manual safety valves at the outlet (at the bottom): discharge valve – 9 for emergency draining and stop valve – 10 for emergency use to prevent unwanted delivery of water to the fFPSC. A manual control valve – 11 has been installed at the outlet of the fFPSC to regulate the volume flow. The volumetric method is used to measure the flow rate, using the lower water tank – 12 with a volume of 50 L. The solar system is vented using an automatic air vent boiler – 13. At the inlet and outlet of the fFPSC, there are ball – 14, 15 and Pt-100 probes – 16, 17. The signal from the Pt-100 probes is detected by an electrical cabinet – 18 located on a stable base (under the fFPSC).

Methods

Measuring chain

The measuring chain, fig. 3, consisted of an experimental installation and a meteorological station, each with the associated measurement equipment to collect the corresponding parameters of the fFPSC. Intensity of solar radiation on the horizontal surface, air temperature, wind speed, the water temperature at the inlet and outlet of the fFPSC, and mass flow rate of water.

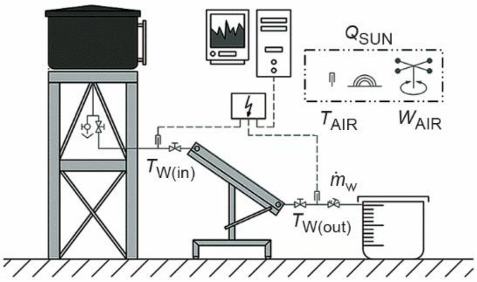

Figure 3. The principle of operation of the experimental installation

The experimental flow (from June to July 2021) was based on the use of hydrostatic pressure, which was the driving force for water flow through the fFPSC. In other words, the potential (gravitational) energy was used to overcome all resistances existing between the upper and lower water tanks.

The upper water tank with float had a double task: to keep the hydrostatic pressure within the desired limits and to provide a sufficient amount of water for the whole experimental day in case of malfunction on the plumbing installations (water tank volume was determined considering that the mass flow of water through the SC should be within the limits of about 0.015 kg/s per m^2 [7]).

The measurement of solar radiation intensity on the horizontal surface, with a time step of five minutes, was performed using a Kipp & Zonen SMP3 Pyranometer. Temperature probes WZP-035 Ø 5 × 50 mm Pt-100 measured water temperatures at the inlet and outlet of the fFPSC synchronously with the operation of the mentioned pyranometer. The accuracies of the used instruments are shown in tab. 2.

Table 2. Devices used accuracy

Device	Accuracy
Kipp & Zonen SMP3 pyranometer	< 5%
Kipp & Zonen data logger METEON	< 0.1%
WZP-035 Ø 5 × 50 mm Pt-100 temperature probes	± 0.2 °C

The flow was regulated by the HERZ STROMAX manual control valve. Initially, the manual control valve was fully closed to fill the installation with water, while simultaneously venting through Caleffi 250 drain pots. Only after the installation was filled with water, the volume (mass) flow was manually adjusted using the scale on the manual control valve.

Fixed flat-plate solar collector thermal performance

Heat power

The heat power of the fFPSC can be determined by the First law of thermodynamics for open thermodynamic systems eq. (1). The specific heat power of the fFPSC is equal to the ratio of its heat power and its active surface, eq. (2):

$$Q_{\mathrm{fFPSC}} = \dot{m}_{\mathrm{W}} c_{\mathrm{W}} [T_{\mathrm{W(out)}} - T_{\mathrm{W(in)}}] \tag{1}$$

$$q_{\mathrm{fFPSC}} = \frac{Q_{\mathrm{fFPSC}}}{A_{\mathrm{fFPSC}}} \tag{2}$$

Solar power

The value of the (total) incident solar heat flux on the fFPSC surface fig. 2 is determined by the direct and diffuse components of solar radiation eq. (3). Since the pyranometer records the value of (total) incident solar radiation on the horizontal surface, according to the Erb's model [34], the diffuse component of solar radiation is calculated by eq. (4), while the direct component by eq. (5) as the difference of (total) incident solar radiation and its diffuse component:

$$Q_{\mathrm{SUN}} = f(H_{\mathrm{DIR}}, H_{\mathrm{DIFF}}) \tag{3}$$

$$H_{\mathrm{DIFF}} = K_{\mathrm{D}} H_{\mathrm{TOT}} \tag{4}$$

$$H_{\mathrm{DIR}} = H_{\mathrm{TOT}} - H_{\mathrm{DIFF}} \tag{5}$$

The ratio of diffuse and total terrestrial solar radiation in eq. (4) is defined by eq. (6) [34]:

$$K_{\mathrm{D}} = f(K_{\mathrm{T}}) = \begin{cases} K_{\mathrm{T}} \le 0.22 \Rightarrow K_{\mathrm{D}} = 1 - 0.09K_{\mathrm{T}} \\ 0.22 < K_{\mathrm{T}} \le 0.8 \Rightarrow K_{\mathrm{D}} = 0.9511 - 0.1604K_{\mathrm{T}} + 4.388K_{\mathrm{T}}^2 - \\ \quad - 16.638K_{\mathrm{T}}^3 + 12.336K_{\mathrm{T}}^4 \\ K_{\mathrm{T}} > 0.8 \Rightarrow K_{\mathrm{D}} = 0.165 \end{cases} \tag{6}$$

The relationship between total terrestrial and total extraterrestrial solar radiation in eq. (6) is defined by eq. (7) [34]:

$$K_{\mathrm{T}} = \frac{H_{\mathrm{TOT}}}{H_{\mathrm{TOT},O}} \tag{7}$$

The value of the specific solar heat power, *i.e.*, the specific solar heat flux, is determined by applying eq. (8):

$$q_{\mathrm{SUN}} = \frac{Q_{\mathrm{SUN}}}{A_{f\mathrm{FPSC}}} \tag{8}$$

Thermal efficiency

Finally, the thermal efficiency of the fFPSC system is the ratio between (specific) thermal and (specific) incident solar heat flux, eq. (9):

$$\eta_{\mathrm{fFPSC}} = \frac{Q_{\mathrm{fFPSC}}}{Q_{\mathrm{SUN}}} = \frac{q_{\mathrm{fFPSC}}}{q_{\mathrm{SUN}}} \tag{9}$$

Results and discussion

Specific heat power and thermal efficiency

The experimental values of the specific incident solar heat flux, specific heat power, and thermal efficiency of the fFPSC, for three days (June 29, June 30, and July 15) during the analyzed period (in 2021), are shown in figs. 4-6.

In the morning and evening of June 29, fig. 4, the intensity of solar radiation was the lowest, as well as the fFPSC specific heat power: 244.34 W/m^2 (09:00 hours), 113.44 W/m^2 (17:00 hours). The solar intensity was highest at 12:35 h (510.5 W/m^2).

On June 30, fig. 5, fFPSC recorded the highest heat power at 12:40 hours (512.68 W/m^2). With the increase in the share of diffuse solar radiation (12:50-13:10 hours, 15:05-15:20 hours, 15:50-16:00 hours, and 16:10-17:00 hours), a decrease in thermal energy generation can be seen (with the following redistribution: 338.15 W/m^2 (12:50-13:10 hours), 248.71 W/m^2 (15:05-15:20 hours), 229.07 W/m^2 (15:50-16:00 hours), and 106.9 W/m^2 (16:10-17:00 hours).

On July 15, fFPSC shows a similar performance to June 29, with a maximum power output of 525.77 W/m^2 (12:45 hours).

The average daily thermal efficiency was within the following limits: 60.67% (June 29), 59.43% (June 30), and 59.85% (July 15). The following maximum values were: 69.96% (10:50 hours, June 29), 69.02% (14:25 hours, June 30) and 70.71% (11:15 hours, July 15).

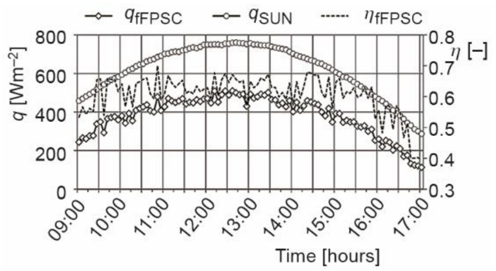

Figure 4. Experimental specific heat power and thermal efficiency for the fFPSC (June 29)

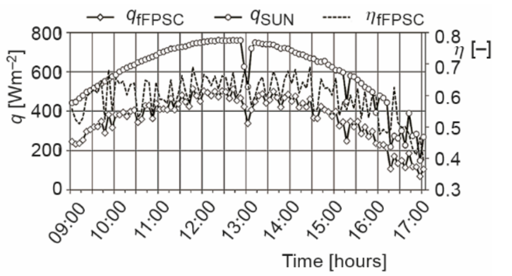

Figure 5. Experimental specific heat power and thermal efficiency for the fFPSC (June 30)

Although the solar curve for all three days, generally, has the shape of a regular parabola, the thermal power does not. The reason for this is the small fluctuations in the mass flow rate, as the float in the upper water tank (despite constant refilling) was not able to keep the hydrostatic pressure constant throughout the day. Also, the presence of dust (a consequence of the wind influence) on the glass surface of the SC, the turbidity of the atmosphere, as well as the discrete influence of the measuring instruments used, must not be disregarded.

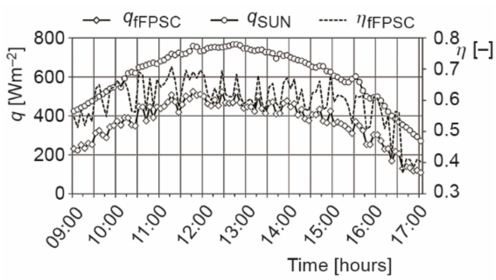

Figure 6. Experimental specific heat power and thermal efficiency for the fFPSC (July 15)

Water characteristic temperature

The daily variations in water temperature at the inlet and outlet of the fFPSC and their differences are shown in figs. 7-9. Although the upper water tank was thermally insulated, fig. 3, the water temperature fluctuated with the change in T_{AIR} and Q_{SUN} (q_{SUN}) as it entered the fFPSC. The phenomena were reflected in the increasing trend of $T_{W(in)}$. On June 29, fig. 7, $T_{W(in)}$ increased from 26.07 °C (09:00 hours) to 36.24 °C (17:00 hours). The same parameter recorded a change from 28.34 °C (start of measurement) to 37.9 °C (end of measurement) on June 30, fig. (8). On the last day of measurement, July 15, fig. (9), the water temperature at the fFPSC inlet varied between 24.29 °C (start) and 32.73 °C (daily maximum, 16:15 hours).

In the case of the outlet temperature $T_{W(out)}$, figs. 7-9, the value of $\dot{m}_W$ had a major influence in addition to the structural and weather conditions. The average daily value of mass flow on all three measurement days was: 0.0058 kg/s (June 29), 0.0069 kg/s (June 30), and 0.0064 kg/s (July 15). All this is reflected in $T_{W(out)}$ as follows: (start, max, stop): June 29 (30.69 °C, 42.95 °C, and 38.39 °C), June 30 (32.26 °C, 42.73 °C, and 39.58 °C), and July 15 (28.25 °C, 38.01 °C, and 33.78 °C).

The water temperature at the outlet of the fFPSC changes as the cloud coverage changes. For example, on June 30, $T_{W(out)}$ dropped from 40.52 °C (12:50 hours) to 37.97 °C (13:00 hours). Similar temperature drops were also recorded at 15:15 hours, 15:55 hours, and 16:35 hours.

External parameters (such are air temperature, wind speed, wind direction, and solar radiation), and internal parameters (such are water inlet temperature, mass flow rate, materials,

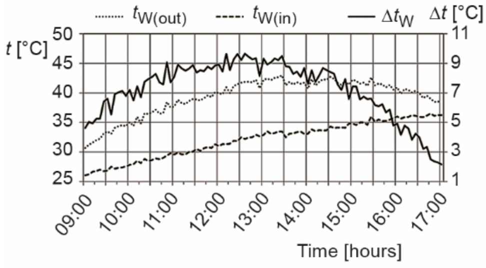

Figure 7. Water characteristic temperatures for the fFPSC (June 29)

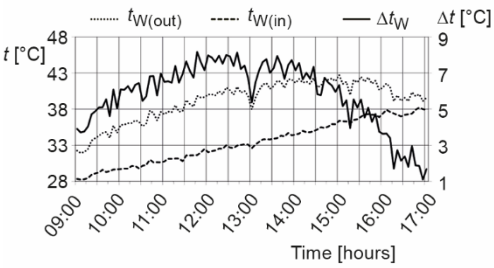

Figure 8. Water characteristic temperatures for the fFPSC (June 30)

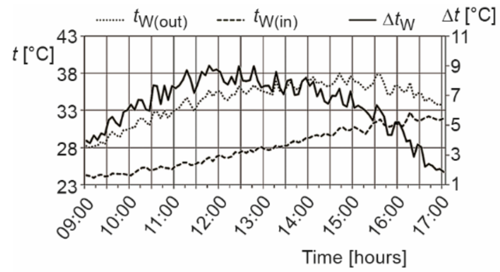

Figure 9. Water characteristic temperatures for the fFPSC (July 15)

and geometry of the fFPSC) affect the ΔT_W value. Each change of these parameters caused a decrease or increase in ΔT_W. In each of the cases studied (June 29, June 30, and July 15), this parameter moved within the following limits: from 2.14 °C (16:55 hours) to 9.65 °C (12:35 hours), from 1.1 °C (16:55 hours) to 8.16 °C (12:40 hours), and from 1.87 °C (17:00 hours) to 9.01 °C (12:45 hours).

Conclusion

The study presented in this paper analyzes the thermal performance of the fFPSC with a selective $Sn\text{-}Al_2O_3$ absorber and gravity water flow.

In the paper, the fFPSC construction with $Sn\text{-}Al_2O_3$ absorber is firstly described in thermal terms. Then the experimental flow and measuring apparatus are described. Research conditions and used thermal equations are also attached. Finally, the results of the investigation of the fFPSC basic thermal parameters with a selective $Sn\text{-}Al_2O_3$ absorber and gravity water flow (heat power, solar power, thermal efficiency, and water characteristic temperatures) for three characteristic summer days during the year 2021 (June 29, June 30, and July 15) are presented.

The factors measured during the experiment (solar radiation on the horizontal surface, wind direction and speed, water temperature at the inlet and outlet, and mass-flow of water) determined the thermal performance of the SC operation, *i.e.* (specific) heat power and thermal efficiency. The average daily (specific) heat power (for the studied period) was: 381.78 W/m^2 (June 29), 364.33 W/m^2 (June 30), and 373.06 W/m^2 (July 15). The average daily thermal efficiency during the same period was: 60.67%, 59.43%, and 59.85%, respectively. These parameters correspond to the variations between inlet and outlet water temperatures: 9.06 °C (June 29, 13:25 hours), 7.46 °C (June 30, 12:40 hours), and 8.69 °C (July 15, 12:25 hours).

Since the world's energy consumption is quite high, ways must be found to reduce it as much as possible. The present study has shown that the use of fFPSC could be relatively beneficial under the conditions of a moderate continental climate. Although the system uses gravity rather than a circulating pump, the water temperature at the outlet can exceed 45 °C depending on weather conditions, and the electricity saved in this way cannot be considered negligible, especially on a global scale. The savings achieved in this way (water heating and gravity flow) could significantly reduce energy dependence and contribute to environmental protection.

Acknowledgment

This investigation is a part of project TR 33015 of the Technological Development of the Republic of Serbia. We would like to thank the Ministry of Education, Science and Technological Development of the Republic of Serbia for their financial support during this investigation.

Nomenclature

A – area, [m^2]
c – specific heat, [Jkg^{-1}K^{-1}]
H – solar radiation, [W]
K_D – diffuse and total terrestrial solar radiation ratio, [–]
K_T – total terrestrial and total extraterrestrial solar radiation ratio, [–]
k – thermal conductivity, [Wm^{-1}K^{-1}]
$\dot{m}$ – mass-flow rate, [kgs^{-1}]
Q – heat flux, [W]
q – specific heat flux, [Wm^{-2}]
T – absolute temperature, [K]
W – wind speed, [ms^{-1}]

Greek symbols

α – absorption coefficient, [–]
β – inclination angle of the fFPSC, [°]
Δ – difference, [°]
δ – thickness, [mm]
ε – emission coefficient, [–]
η – efficiency, [–]
τ – transparency coefficient, [–]

Subscripts

AIR – air
DIFF – diffuse
DIR – direct
In – inlet
O – extraterrestrial
Out – outlet
SUN – solar
TOT – total
W – water

Acronyms

FPSC – flat-plate SC
fFPSC – fixed FPSC
ETSC – evacuated tube SC
SC – solar collector

References

[1] ***, International Energy Agency (IEA), https://www.iea.org
[2] Yousefi, Y., *et al.*, Energy Efficiency in Educational Buildings in Iran: Analysis and Measures, *Proceedings, 1* (2015), 1, pp. 169-174
[3] ***, Energadata, https://www.enerdata.net
[4] ***, Statista, https://www.statista.com
[5] Ibrahim, A., Kocak, S., Theoretical Energy and Exergy Analyses of Solar Assisted Heat Pump Space Heating System, *Thermal Science*, *18* (2014), 2, pp. 417-427
[6] Solanki, A., Yash, P., Applications of a Flat Plate Collector in Dairy Industries: A review, *International Journal of Ambient Energy*, *43* (2022), 1, pp. 1915-1923
[7] Lukic, N., Babić, M., *Solar Energy* (in Serbian), Faculty of Engineering, Kragujevac, Serbia, 2008
[8] Wazwaz, A., *et al.*, Solar Thermal Performance of a Nickel-Pigmented Aluminium Oxide Selective Absorber, *Renewable Energy*, *27* (2002), 2, pp. 277-292
[9] Wazwaz, A., *et al.*, The Effects of Nickel-Pigmented Aluminium Oxide Selective Coating Over Aluminium Alloy on the Optical Properties and Thermal Efficiency of the Selective Absorber Prepared by Alternate and reverse Periodic Plating Technique, *Energy Conversion and Management*, *51* (2010), 8, pp. 1679-1683
[10] Li, Z., *et al.*, Aqueous Solution-Chemical Derived Ni-Al_2O_3 Solar Selective Absorbing Coatings, *Solar Energy Materials & Solar Cells*, *105* (2012), Oct., pp. 90-95
[11] Xue, Y., *et al.*, Spectral Properties and Thermal Stability of Solar Selective Absorbing AlNi-Al_2O_3 Cermet Coating, *Solar Energy*, *96* (2013), Oct., pp. 113-118

[12] Teixeira V., *et al.*, Spectrally Selective Composite Coatings of Cr-Cr_2O_3 and Mo-Al_2O_3 for Solar Energy Applications, *Thin Solid Films*, *392* (2001), 2, pp. 320-326
[13] Xinkang, D., *et al.*, Microstructure and Spectral Selectivity of Mo-Al_2O_3 Solar Selective Absorbing Coatings After Annealing, *Thin Solid Films*, *516* (2008), 12, pp. 3971-3977
[14] Antonaia, A., *et al.*, Stability of W-Al_2O_3 Cermet Based Solar Coating for Receiver Tube Operating at High Temperature, *Solar Energy Materials & Solar Cells*, *94* (2010), 10, pp. 1604-1611
[15] Ding, D., *et al.*, Optical, Structural and Thermal Characteristics of Cu-$CuAl_2O_4$ Hybrids Deposited in Anodic Aluminum Oxide as Selective Solar Absorber, *Solar Energy Materials & Solar Cells*, *94* (2010), 10, pp. 1578-1581
[16] Nuru, Z. Y., *et al.*, Pt-Al_2O_3 Nanocoatings for High Temperature Concentrated Solar Thermal Power Applications, *Physica B: Condensed Matter*, *407* (2012), 10, pp. 1634-1637
[17] Barshilia, H. C., *et al.*, Structure and Optical Properties of Ag-Al_2O_3 Nanocermet prepared Solar Selective Coatings using unbalanced magnetron sputtering, *Solar Energy Materials & Solar Cells*, *95* (2011), 7, pp. 1707-1715
[18] Chorchong, T., *et al.*, Characterization and Spectral Selectivity of Sn-Al_2O_3 Solar Absorber, *Key Engineering Materials*, Trans Tech Publications Ltd, *675* (2016), Jan., pp. 467-472
[19] Wamae, W., *et al.*, Influence of Tin Content on Spectral Selectivity and Thermal Conductivity of Sn-Al_2O_3 Solar Selective Absorber, *Materials for Renewable and Sustainable Energy*, *7* (2018), 1, pp. 1-8
[20] Wamae, W., *et al.*, Thermal Efficiency of a New Prototype of Evacuated Tube Collector using Sn-Al_2O_3 as a Selective Solar Absorber, *Walailak Journal of Science and Technology*, *15* (2018), 11, pp. 793-802
[21] Deng, Y., *et al.*, Experimental Study of the Thermal Performance for the Novel Flat Plate Solar Water Heater with Micro Heat Pipe Array Absorber, *Energy Procedia*, *70* (2015), May, pp. 41-48
[22] Fan, M., *et al.*, Comparison of Different Dynamic Thermal Performance Prediction Models for the Flat-Plate Solar Collector with a New V-Corrugated Absorber, *Solar Energy*, *204* (2020), July, pp. 406-418
[23] Bezaatpour, M., Rostamzadeh, H., Simultaneous Energy Storage Enhancement and Pressure Drop Reduction in Flat Plate Solar Collectors Using Rotary Pipes with Nanofluid, *Energy and Buildings*, *239* (2021), May, 110855
[24] Seddaoui, A., *et al.*, Performance Investigation of a New Designed Vacuum Flat Plate Solar Water Collector: A Comparative Theoretical Study, *Solar Energy*, *231* (2022), Jan., pp. 936-948
[25] Garcia, R. P., *et al.*, Thermal Efficiency Experimental Evaluation of Solar Flat Plate Collectors when Introducing Convective Barriers, *Solar Energy*, *182* (2019), Apr., pp. 278-28
[26] Eltaweel, M. *et al.*, Indirect Thermosiphon Flat-Plate Solar Collector Performance Based on Twisted Tube Design Heat Exchanger Filled with Nanofluid, *International Journal of Energy Research*, *44* (2020), 6, pp. 4269-4278
[27] Michael, J. J., Iniyan. S., Performance of Copper Oxide-water Nanofluid in a Flat Plate Solar Water Heater Under Natural and Forced Circulations, *Energy Conversion and Management*, *95* (2015), May, pp. 160-169
[28] Prasad, M., Chandra. K. S., Optimum Tilt of Solar Collector for Maximum Natural Flow, *Energy Conversion and Management*, *30* (1990), 4, pp. 369-379
[29] Varol, Y., Hakan, F. O., A Comparative Numerical Study on Natural Convection in Inclined Wavy and Flat-Plate Solar Collectors, *Building and Environment*, *43* (2008), 9, pp. 1535-1544
[30] Taner, T., Optimisation Processes of Energy Efficiency for a Drying Plant: A Case of Study for Turkey, *Applied Thermal Engineering*, *80* (2015), Apr., pp. 247-260
[31] Taner, T., Sivrioglu, M., A Techno-Economic & Cost Analysis of a Turbine Power Plant: A Case Study for Sugar Plant, *Renewable and Sustainable Energy Reviews*, *78* (2017), Oct., pp. 722-730
[32] Taner, T., A Feasibility Study Of Solar Energy-Techno Economic Analysis from Aksaray City, Turkey, *Journal of Thermal Engineering*, *3* (2019), 5, pp. 1-1
[33] Djurdjevic, D. Z., Perspectives and Assessments of solar PV Power Engineering in the Republic of Serbia, *Renewable and Sustainable Energy Reviews*, *15* (2011), 5, pp. 2431-2446
[34] Kalogirou, S. A., Solar Thermal Collectors and Applications, *Progress in energy and combustion science*, *30* (2004), 3, pp. 231-295

Paper submitted: September 4, 2022
Paper revised: October 10, 2022
Paper accepted: October 17, 2022